Sequential onset and concurrent expression of miR-9 genomic loci in single cells contributes to the temporal increase of mature miR-9 in zebrafish neurogenesis

Soto, X.[1], Minchington, T.[1], Lea, R.[1], Lee, J.[2] and Papalopulu, N[1]*

*correspondence: nancy.papalopulu@manchester.ac.uk

[1]Division of Developmental Biology and Medicine, School of Medical Sciences, Faculty of Biology Medicine and Health, The University of Manchester, Oxford Road, Manchester, M13 9PT, UK;

[2]Medicines Discovery Catapult, Block 35, Mereside, Alderley Park, Alderley Edge, Cheshire, SK10 4TG, UK

Abstract

Gene expression oscillations of the Hes/Her family members of transcriptional repressors are important for cell state transitions during neural development. The input of miR-9 is necessary to constrain gene expression noise, allowing oscillations to occur and to be decoded by downstream genes. Hes/Her dynamics are sensitive to the amount of miR-9 present in the cell but the mechanism by which miR-9 is quantitatively controlled is not known. In vertebrates, there are several distinct genomic loci that produce the same mature miR-9, leading to a number of possibilities of how the production of mature miR-9 may be regulated.

Here, we show that the expression of miR-9 increases spatially and temporarily over zebrafish development. A detailed time course of the expression of 7 pri-miR-9 genomic loci shows that they have distinct temporal and spatial profiles, which may be brought about by different numbers of E/N-boxes in their regulatory regions. Focusing on pairs that are expressed in the same area of the hindbrain region, namely pri-miR-9-1/pri-miR-9-4 and pri-miR-9-1/pri-miR-9-5, we find that they sequentially activated during neurogenesis, concurrent with a known change in Her6 dynamics from noisy to oscillatory. Analysis of expression at the single-cell level shows that although they are sequentially activated, early and late pri-miRs are mostly concurrently transcriptionally active in the same cells. This finding supports the idea that increased mature miR-9 is contributed, at least in part, by overlapping activation of distinct loci. We propose that this may lead to an additive, sharp, increase of mature miR-9 which in turn may lead to rapid changes in Her6 dynamics.

Introduction

MicroRNAs are a class of small (~22 nucleotides) regulatory non-coding RNAs, which regulate gene expression at the post-transcriptional level. These small RNAs are processed from large microRNA primary transcripts (pri-miRs) into 70~90nt precursors (pre-miRs) before further splicing into ~22nt mature microRNA. miR-9 is a highly conserved microRNA which is expressed predominantly in the central nervous system (CNS) of vertebrates and plays a crucial role during CNS development.

Previous work in xenopus, zebrafish and mice has shown that miR-9 is essential for the correct timing of cell fate transitions during neurogenesis (Coolen et al., 2013) (Bonev et al., 2011; Bonev et al., 2012). miR-9 post-transcriptionally targets many transcription factors that are involved in neural development such as FoxG1 (Shibata et al., 2008), Tlx (Zhao et al., 2009) and members of the Hes/Her helix-loop-helix family of transcription factors, including Hes1 in mouse and Xenopus (Bonev et al., 2011; Bonev et al., 2012) and Her6 in zebrafish (Coolen et al., 2012; Galant et al., 2016; Soto et al., 2020).

The Hes/Her family of proteins are expressed dynamically in an oscillatory manner at the ultradian timescale (Hirata et al., 2002; Shimojo et al., 2008). Hes/Her oscillations are achieved by a negative feedback loop, whereby Hes/Her proteins inhibit their own transcription coupled with a rapid turnover of protein and mRNA. Instability of both protein and mRNA allows for levels of the protein to fall, de-repression to occur and expression to resume, generating a cyclic pattern (Hirata et al., 2002; Novak and Tyson, 2008). Indeed, both mRNA and protein of Hes family

genes are unstable, for example, in mice, the half-life of *Hes1* mRNA is ~24 minutes and the HES1 protein half-life is in the order of 22 minutes (Hirata et al., 2002) and the Her6 (Zebrafish orthologue) protein half-life is around 10 minutes (Soto et al., 2020).

The instability of the mRNA, as well as the translation of the protein, are controlled by microRNAs. Indeed, our previous work revealed that miR-9 regulation is important for allowing the oscillatory pattern of expression of HES1 to emerge. However, the amount of miR-9 is important as too much or too little miR-9 can lead to dampening of HES1 oscillations (Bonev et al., 2012; Goodfellow et al., 2014). We have also recently shown that in zebrafish, the dynamics of Her6 protein expression switch from noisy to oscillatory and this coincides temporally with the onset of miR-9 expression in the hindbrain (Soto et al., 2020). Furthermore, when the influence of miR-9 on *her6* is removed experimentally, Her6 expression does not evolve away from the “noisy” regime with a consequent reduction in progenitor differentiation. We have interpreted this to mean that the miR-9 input is necessary to constrain gene expression noise, enabling oscillations to occur and to be decoded by downstream genes (Soto et al., 2020). Together these findings support that Hes/Her dynamics are sensitive to the amount of mature miR-9 present in the cell, however, the mechanism by which this is controlled is not known.

The question is complicated by the observation that vertebrates (and some invertebrates) possess multiple copies of the miR-9 gene at distinct loci but all capable of producing the same mature microRNA. For example, both human and mouse contain 3 copies of miR-9 (Rodriguez-Otero et al., 2011; Shibata et al., 2011)

and frogs have 4 (Walker and Harland, 2008). Due to an additional round of whole-genome duplications in teleost fish (Amores et al., 1998; Jaillon et al., 2004), zebrafish have 7 paralogues of miR-9 (miR-9-1 to miR-9-7) (Chen et al., 2005).

One possibility is that different genomic loci contribute to miR-9 regulation in a qualitative way, that is due to differential temporal and spatial specificity of mature miR-9 expression. Indeed, there is some limited evidence that these discrete copies of miR-9 are expressed differentially during development both temporally and spatially (Nepal et al., 2016; Tambalo et al., 2020). Another, and yet unexplored, possibility is that transcription from different loci may serve to control miR-9 quantitatively, that is to increase the amount of miR-9 in the cell and perhaps do so in a temporally controlled manner.

Here, we undertake a systematic study of pri-miR-9 expression in zebrafish that aims to address the likelihood of these distinct scenarios, with special attention to the possibility of a quantitative control mechanism. We show by *in situ* hybridization that the amount of mature miR-9 increases over zebrafish development, spreading from the forebrain to the hindbrain between 24 and 48hpf. A detailed time course of the expression of all 7 pri-miR-9 paralogues shows that they are all transcriptionally active, but exhibit subtle, yet distinct, temporal and spatial profiles which could be contributed by differences in their regulatory regions, for example, correlating with the number of E/N-boxes present in the proximal promotor of each pri-miR-9. Focusing on 2 pairs of early and late expressed pri-miR-9s, (pri-miR-9-1 and pri-miR-9-4, or pri-miR-9-5) by fluorescent in situ hybridization at single cell level, we find that, surprisingly, in some cells early and late pri-miR-9s were concurrently

transcriptionally active. Taken together, we find evidence for a qualitative mechanism in the deployment of pri-miR-9s, as well as a previously un-appreciated quantitative component, both of which may contribute to the decoding function of mature miR-9s.

RESULTS

All pri-mir-9s are expressed but with differed temporal onset

To investigate the expression of the mature miR-9 in zebrafish embryos, we first performed a whole mount in situ hybridization (WM-ISH) for the mature miR-9 using an LNA (locked nucleic acid) probe. Mature miR-9 was detected only in forebrain at 24hpf (**Fig. 1a**) while at 30hpf miR-9 was observed in the midbrain and in rhombomere 1 (r1) of the hindbrain (hb), maintaining high expression in forebrain (**Fig. 1a**, 30hpf-red head arrow). Later in development miR-9 expression was seen in the posterior hindbrain (**Fig. 1a**, 34-36hpf-blue arrow). As development progressed, increased levels of expression throughout the hindbrain were observed while expression in the forebrain decreased (**Fig. 1a**, 48hpf, blue arrow: hindbrain, green arrow: forebrain). These results show a temporally controlled antero-posterior wave of miR-9 expression along the brain/hindbrain axis.

In zebrafish, the mature miR-9 can be produced from seven paralogous of miR-9. The miR-9 paralogues occupy 7 unique loci across the genome (GRCz11; Genome Reference Consortium Zebrafish Build 11) (Yates et al., 2020). With the exception of miR-9-3 which is located upstream of a lincRNA, all miR-9 genes are intragenic, overlapping annotations of lincRNAs or proteins(Yates et al., 2020) (**Figure S1a,b**). Our *in silico* analysis of previously published RNA-seq data confirms the differential temporal expression of six of the seven miR-9 paralogues host genes (White et al.,

2017). It is also clear that expression of miR-9 host genes coincides with a gradual decline in the expression of Her/Hes family genes expression, consistent with the idea that *hes/her* genes are major targets of miR-9 (**Figure S1c**) (Bonev et al., 2011).

Previous work has revealed that the 7 miR-9 zebrafish paralogues are expressed in forebrain at early stages of neurogenesis while toward the end are also expressed in hindbrain (Nepal et al., 2016). However, little is known about the period spanning the peak of neurogenesis, when miR-9 controls downstream targets such as the ultradian oscillator Her6. To characterize the expression in greater spatiotemporal detail, particularly over the hindbrain area where Hes/Her target genes are expressed, we investigated the nascent expression of all 7 precursors over a time period spanning the peak of neurogenesis which occurs at 33hpf (Lyons et al., 2003) using specific probes for each pri-miR-9 (**Figure S2; Methods**, Molecular cloning).

We observed that all pri-miR-9s were first expressed in the forebrain (24hpf), in a regional specific manner, which was not further characterised here. At 48hpf they are all also expressed in hindbrain (**Fig. 1b,d**, 24 and 48hpf and **Figure S3a-c**) consistent with what has been described before (Nepal et al., 2016). Differential expression was evident in the intermediate stages. Specifically, pri-miR-9-3, 9-4 and 9-5 were expressed ahead of the others in the hindbrain. Here, pri-miR-9-4 was evenly and highly expressed while pri-miR-9-3 and pri-miR-9-5 were expressed in a gradient from anterior to posterior (**Fig. 1b,c**; 30hpf; blue arrowhead). At the peak of hindbrain neurogenesis (34-36hpf), pri-miR-9-2 and pri-miR-9-7 were upregulated, joining most of the pri-miR-9s that were highly expressed at this stage (**Fig. 1b**, 34-

36hpf). Pri-miR-9-1 and miR-9-6 were temporally delayed until 48hpf, at which point all pri-miR-9 were fully expressed.

Thus, overall, every pri-miR-9 was expressed in the CNS and exhibited similar but unique expression patterns and a temporal progression. Characterising the temporal order of the onset of expression in intermediate stages was a first step in asking whether the expression of different pri-miR-9s is distinct or additive in the hindbrain, which we address below.

Partially overlapping spatial expression of early pri-miR-9s

We selected three different precursors based on the onset of their hindbrain temporal expression during development, earliest or latest, and the phylogenetic analysis of precursors sequences in clades/subgroups performed by Alwin Prem Anan et al., 2018. Pre-miR-9-1 was selected as the latest to express in the hindbrain belonging to clade I/subgroup II, pre-miR-9-5 as the earliest to express that belongs to clade I/subgroup I and pre-miR-9-4 as the earliest, belonging to clade II (Alwin Prem Anand et al., 2018) (**Figure S3d**).

Double WM-FISH for pri-miR-9-1 and pri-miR-9-4 performed on stage 32hpf embryos revealed expression of pri-miR-9-4 along the antero-posterior hindbrain axis, while pri-miR-9-1 expression was limited to the region of the anterior hindbrain corresponding to rhombomere 1 (**Fig. 2a**, red arrows). The transversal view of rhombomere 4 reveals expression of pri-miR-9-4 within the ventricular zone, while pri-miR-9-1 was almost completely absent (**Fig. 2d, f**). These data indicate that pri-miR-9-s are mainly expressed in the region where most of the dorsal progenitors,

medial progenitors and ventral progenitors are found (**Fig. 2f**) (Lyons et al., 2003; Tambalo et al., 2020). The double WM-FISH experiment was repeated with pri-miR-9-1 and pri-miR-9-5. At 32hpf, pri-miR-9-5 is evenly distributed antero-posteriorly in the hindbrain whilst pri-miR-9-1 was mostly expressed in rhombomere 1 as one would expect due to the delayed onset of expression for pri-miR-9-1 (**Fig. 2b**, red arrows). Fluorescent intensity quantification of the region of interest (**Fig. 2a,b** merge, yellow rectangle) show variability in the levels of expression, pri-miR-9-4 and pri-miR-9-5 are significantly high expressed ($P<0.05$ and $P<0.0001$, respectively) to pri-miR-9-1 (**Fig. 2c),** supporting the hypothesis of pri-miR-9-4 and pri-miR-9-5 early expression. Transversal imaging of pri-miR-9-1/pri-miR-9-5 revealed similar pattern expression to pri-miR-9-1/pri-miR-9-4 analysis. Interestingly, subtle differences were observed in pri-miR-9-4 which had a broader pattern of expression, extending further in the dorsal progenitor area than pri-miR-9-5 indicating some differences in spatial expression between pri-miR-9s of the same temporal profile (**Fig. 2d-e**, compare middle panels, **Fig. 2f**).

Progressive additive expression of pri-miR-9s

In order to examine whether the late expression of pri-miR-1 is cumulative with pri-miR-4 and pri-miR-5, or whether it is spatially distinct, we analysed expression at later stages. Coronal and transversal views of pri-miR-9-1 double WM-FISH with pri-miR-9-4 and pri-miR-9-5 revealed both overlapping and distinct expression of the primary transcripts (**Fig. 3a-d**). Distinct expression was most clearly observed in transversal views that show pri-miR-9-5 is more restricted in its expression to the middle-ventral progenitor region of the ventricular zone, while pri-miR-9-1 was more broadly expressed toward the dorsal progenitor region (**Fig. 3d, e**). In order for the

overlapping expression to contribute to the total levels of mature miR-9 in a cell, early and late pri-miR-9s would need to be expressed in the same cells, which was examined next.

Total mature miR-9 is contributed by overlapping activation of distinct miR-9 loci

To investigate the existence of a spatiotemporal overlap in pri-miR-9 expression at the single cell level, we performed double WM-FISH for pri-miR-9-1 with pri-miR-9-4 and pri-miR-9-5. Cell boundaries were visualized with the cell boundary marker BODIPY-texas red (BP-TR). At 48hpf we observed cells that have only one miR-9 precursor present (**Fig. 4c,d,g,h**) from which, cells expressing only pri-miR-9-1 were often found in the dorsal progenitor region of the ventricular zone (**Fig. 4a,c,e,g**) while cells expressing only pri-miR-9-4 or pri-miR-9-5 and not pri-miR-9-1 were mostly observed in the middle-ventral progenitor region of the ventricular zone (**Fig. 4a,d,e,h**) suggesting differential spatial expression. However, we also found many cells co-expressing two pri-miR-9s (**Fig. 4a,b,e,f**), suggesting that different miR-9 paralogues are concurrently transcriptionally active in the same cells.

Diverse regulation of miR-9 promoters

To have a better understanding of the origin of these spatial and temporal expression differences, we focused on the transcriptional activation/repression/regulation of the different miR-9 precursors. Transcriptional repressors such as Hes/Her family can inhibit expression through the binding to N/E-boxes (Akazawa et al., 1992; Sasai et al., 1992). An E-box (enhancer box) is a DNA

response element that can act as a protein-binding site of an activator or repressor, while an N-box is a protein-binding for a repressor such as Hes1(Sasai et al., 1992).

We first performed an *in-silico* analysis to identify putative canonical DNA binding motif of the bHLH transcription factors (E-boxes), with consensus sequence CANNTG, in a 2kb region upstream and 1kb region downstream of the transcriptional start site of the transcripts of the miR-9 paralogues as previously defined in Chirag et al. 2016. We found miR-9-2 and miR-9-4 promotor/proximal enhancer region contained the highest number of putative E-boxes, 21 and 18, respectively, followed by miR-9-3, 5, 7, 1 and 6 (**Fig. 5a, b**). In concordance, the bHLH transcription factor Neurogenin1 (Ngn1) is a pro-neural gene known to induce miR-9 thus is a potential candidate to promote differential temporal expression of the seven miR-9 paralogues through E-box binding (Zhao et al., 2015)

We next performed *in silico* analysis of the DNA binding motif sequence CACNAG called, N-box. As previously mentioned, the transcription of miR-9 precursors is repressed by Hes1 protein through this binding site (Bonev et al., 2012; Sasai et al., 1992). We identified variability within host gene regulatory sequences; 9 putative N-boxes were found in miR-9-5, 5 N-boxes in miR-9-2, 3 N-boxes in miR-6 while only 1 in miR-9-7, in miR-9-4 and miR-9-1 and none in miR-9-3 (**Fig. 5a, b**). These results may reflect variability of Hes1 strength regulation over the miR-9s proximal promotor dependent on the number of N-boxes that each miR-9 promoter/proximal enhancer region contains. Indeed, we observed that expression levels of pri-miR-9-5 is consistently reduced (**Fig. 5e**. dashed line) in the regions where the zebrafish Hes1 orthologues, Her6/Her9, are highly expressed (**Fig. 5c**. her6/her9 merge-white

underlined), corresponding to the medial-dorsal progenitor region of the ventricular zone and pri-miR-9-1 is expressed more broadly, with expression in the dorsal progenitor region of the ventricular zone. We also observed expression of pri-miR-9-4 narrowed to the ventral progenitor region of the ventricular zone (**Fig. 5d**, dashed line), this can be explained by its higher number of E-boxes when compared to pri-miR-9-1. Combined, these data outline the dynamical spatial expression of the highly conserved microRNA, miR-9, based on the ability of repressors/activators to modulate the different promoters of the seven different mir-9 precursors.

Discussion

miR-9 is expressed from several genomic loci which, after transcription and processing, produce the same 5' mature form of miR-9 which is particularly interesting because it targets the key neural progenitors Her/Hes TFs. How common is this multi-locus organisation? In humans 6.3% of mature microRNA arms are identical across two or more loci (Kozomara et al., 2019), thus, it is not very common, but it is not unique to miR-9. In zebrafish this number rises to around 32.3% (Kozomara et al., 2019). The higher number of microRNA expressed from multiple loci is possibly due to the teleost-specific whole-genome duplication (WGD). Evidence from rainbow trout also shows that following the salmonid-specific extra round of WGD, microRNAs appear to be retained at higher levels than protein-coding genes (Berhelot et al 2014). This may suggest that extra copies of microRNA are evolutionary advantageous but why this is the case was not understood. Here, we propose that retention of multiple microRNA loci could have specific functional advantages for regulatory control of target gene expression of an organism.

By examining in detail the temporal and spatial expression at single cell level of 3 select early and late pri-miR-9s, we offer two possible explanations for this multi-site organisation or primary transcripts.

The first explanation involves a qualitative mechanism. In this scenario, distinct pri-miR-9s have different spatial expression, which allows them to target different, i.e. region-specific, genes. Some of the differences in the spatial expression of pri-miR-9s are easily discernible macroscopically (e.g. differential expression in the forebrain) while others are subtle and require post-hybridisation sectioning to document, as we have done here. An example of the latter is the expression of pri-miR-1 which extents more dorsally in the hindbrain than pri-miR-4. This correlates well with the expression of her6 and her9, which are both miR-9 targets but are expressed adjacent to each other along the D-V axis (Soto et al. 2020).

The second explanation favours a quantitative mechanism. In this scenario, the differential temporal expression, where some primary transcripts commence their expression early while others are only expressed late, results in the simultaneous expression of both (or more) transcriptional loci in the same cells at a particular time in development. In support of this scenario, we have shown by FISH that pri-miR-9-1, a late onset pri-miR-9, is co-expressed in the same cells as the earlier onset pri-miR-9-4 or -5. Interestingly, we have not seen evidence for a mechanism where one pri-miR-9 switches off and another one comes on, arguing against a mechanism where an early pri-miR-9 “passes on” the task of repression to a later expressed one; rather all loci seem to remain active at least for the duration of our observations which covers the period of embryonic neurogenesis. This means that both early and

late pri-miR-9s are concurrently transcribed at late stages, and assuming they are both processed the amount of mature miR-9 in a cell could sharply increase. Given that transcription saturates easily in many systems (Hafner et al., 2020), this co-expression may be a strategy to increase the amount of miR-9 available to the cell than what is possible with transcription from one locus alone. Indeed, we have shown that the dynamical regime of Hes1 (i.e. oscillatory expression to stable expression at different levels) as well as the amount of time that Hes1 oscillates for, depends on the amount of miR-9 in the cell (Bonev et al., 2012; Goodfellow et al., 2014). More recently, we have shown by in vivo manipulations, that the input of miR-9 changes the dynamic expression of her6 from noisy to oscillatory (Soto et al., 2020).

Like many other miRs, miR-9 has been shown to be quite stable in xenopus and was thus presumed to accumulate gradually over time (Bonev et al., 2012; Goodfellow et al., 2014). In turn, changing the levels of miR-9 in the cell would drive the dynamics of Hes1 from one dynamical regime to another, as described above. While more recent studies have questioned the long stability of miRs by using different methods and showing that the stability of miR-9 varies between tissues (Kim et al., 2020; Marzi et al., 2016; Ruegger and Grosshans, 2012), the onset of additive transcription from two loci is nevertheless likely to exert a sharp increase in the amount of miR-9 present in the cell. It is possible that some genes/networks do not respond to slow increases of miR-9 (a form of adaptation observed in signalling pathways (Dessaud et al., 2007)), and a sharp, non-linear, increase may be needed to push a dynamical system into a new state associated with a cell fate change. In fact, non-linearity of

reactions is a key feature of systems that can generate oscillatory gene expression (Novak and Tyson, 2008).

The qualitative and quantitative mechanisms suggested above are not mutually exclusive and may be combined and also take place at the same time. A common element is that both mechanisms would rely on distinct control of expression of different miR-9 loci. In support of this, we have found that characteristics of the regulatory regions and the organisation of pri-miR-9 in their host transcriptional units show some distinct features. Interestingly, some of the regulatory region differences may also be quantitative rather than simply qualitative; Indeed, we have found a difference in the number of repressive N-boxes but also differences in the number of activators E-boxes, which may correlate with the differences in the extent of medio-lateral (ontogenetically ventral-dorsal) expression of some pri-miR-9 pairs. Another common element is that in both scenarios, a sequential temporal order of activation can be involved, and indeed, we have observed a temporal sequence of activation for most pri-miR-9s, roughly starting anteriorly and spreading posteriorly. This temporal order was also observed when considering the entire miR-9 family and the Her gene targets which were expressed on the whole earlier and were downregulated when pri-miR-9s were upregulated.

Where multiple paralogues of a microRNA are present, differential qualitative and quantitative regulation may be a more common feature than is currently appreciated. In this respect, it is interesting that a recent study found that miR-196 paralogues show both unique and overlapping expression. Single KOs showed some redundancy but importantly, they also showed unique phenotypes and combinatorial

KOs showed better penetrance together with additional defects, suggesting an additive role of miR-196 paralogues in establishing vertebral number (Wong et al., 2015).

In conclusion, by providing evidence for both a quantitative and qualitative mechanism, we have made conceptual advances on the possible roles of organising pri-miR-9s in several distinct genomic loci, which may have led to their evolutionary conservation. In addition, we highlight here some practical benefits of our work for the experimenter; once mature miR-9 has been produced, it is not possible to tell which genomic locus it was transcribed from. Thus, with multiple such loci being potentially involved, it is very difficult for the experimenter to select the correct one to tag, mutagenize or otherwise manipulate by CRISPR/Cas9. Therefore, an added benefit of our work is that the detailed characterisation we have described here will enable the selection of the correct genomic locus for genetic manipulation of miR-9 production, depending on the precise research question.

Acknowledgements

We are grateful to Dr Laure Bally-Cuif for sharing plasmids. The authors would also like to thank the Biological Services Facility, Bioimaging and Systems Microscopy Facilities of the University of Manchester for technical support. This work was supported by a Wellcome Trust Senior Research Fellowship to NP (090868/Z/09/Z). The funders had no role in study design, data collection and analysis, decision to publish, or preparation of the manuscript.

Author Contributions

Conceptualization, X.S. and N.P.; Methodology, X.S. and N.P; Software, T.M. and X.S.; Validation, X.S., T.M and R. L.; Formal Analysis, X.S. and T. M. ; Investigation, X.S., R.L, J. L. and T.M.; Resources, N.P. and X.S.; Data Curation, X.S. and T.M..; Writing - Original Draft, X.S.; Writing – Review & Editing, N.P., X.S. and T.M..; Visualization, X.S., T.M and R.L.; Supervision, N.P. and X.S; Project Administration, N.P and X.S.; Funding Acquisition, N.P.

Declaration of Interests

The authors declare no competing interests.

Methods

Research Animals

Animal experiments were performed under UK Home Office project licenses (PFDA14F2D) within the conditions of the Animal (Scientific Procedures) Act 1986. Animals were only handled by personal license holders.

mRNA extraction and Quantitative real-time PCR (qRT-PCR)

mRNA was extracted using Trizol from a pool of 10 zebrafish embryos. SuperScript II (Invitrogen) was used to do reverse cDNA synthesis using hexamer primers. For quantitative real-time PCR (qRT-PCR) cDNA samples were diluted to a concentration of 50 ng/µl with dH_20. Each qPCR reaction was prepared in triplicate in a 96-well plate with each well consisting of 0.2 µM each forward and reverse primer, 50ng cDNA and SYBR Green Mastermix (ThermoFisher). Zebrafish embryo Reactions were run on Step One Plus Real-time PCR System (Applied Biosystems) alongside negative controls. The data for each sample was normalized to the expression level of *b-actin* and analysed by the $2^{-\Delta\Delta Ct}$ method, normalized to miR-9-1 expression. For each primer pair, the PCR product was examined by gel

electrophoresis and its melting curve to ensure a single fragment of the predicted molecular weight.

Molecular cloning

RNA probes for pri-miR-9-1, pri-miR-9-2, pri-miR-9-4, pri-miR-9-5 and pri-miR-9-7 were PCR amplified and cloned into pCRII vector using primers described in **Table S1**. Except for pri-miR-9-2 probe, they were designed to distinguish the primary transcripts by including sequences, intron and exon, before and after each microRNA processing, while also covering the sequence corresponding to mature miR-9 **(Figure S2)**. Since the mature miR-9 sequence is conserved between paralogs, to avoid any cross-binding of probes to this sequence we mutated it on each probe by using QuikChange II XL Site-Directed Mutagenesis assay. This allowed us introduce deletions and single nucleotide exchange in specific regions of the mature miR-9 sequence (**Table S2**; **Figure S2**; sequence highlighted in red).

pri-miR-9-3 and pri-miR-9-6 probes were generated from plasmids kindly gifted by Laure Bally-Cuif (Nepal et al., 2016).

Whole mount chromogenic and fluorescence *in situ* hybridization and sectioning

Chromogenic *in situ* hybridisation was performed as previously described by Christine Thisse (Thisse and Thisse, 2008). Multicolour fluorescence *in situ* hybridisation was modified from Hoppler and Vize (Lea et al., 2012) by developing with tyramide amplification (Perkin Elmer) after addition of antisense RNA probes and antibodies conjugated to horseradish peroxidase (Lea et al., 2012).

Sections were obtained as described in Dubaissi (Dubaissi et al., 2012) with modifications. Embryos were embedded in 25% fish gelatine and 30% sucrose for a minimum of 24 hrs. 18µm thickness hindbrain sections were collected and transferred onto superfrost glass slides. The slides were air dried overnight under the fume hood and stained with 5µM BODYPI-TR (Thermo-Fisher Scientific) before mounting with Prolong Diamond Antifade.

Imaging

Chromogenic *in situs* were imaged using a Leica M165FC with a DFC7000T camera. Fluorescent *in situ* sections were imaged using Leica TCS SP5 upright confocal with HCX PL APO CS 40.0x1.25 OIL UV lens or Olympus FLUOVIEW FV1000 confocal with UPLSAPO 20X NA:0.75 lens or UPLSAPO 20X NA:0.75 lens.

Expression analysis of hes/her genes and microRNA hosts

For the *in silico* analysis of the microRNA host gene expression we downloaded the time course RNA-seq data (TPM) from White et al. 2017 supplemental file 3. Here we used the overlapping host genes as a proxy for the expression of the microRNA. MicroRNA would not show up in standard RNA-seq analysis and there is no current microRNA time course data. Host genes were identified as those with overlapping annotations with the miR-9 genes. The host genes for each microRNA are in **Table S4**. MiR-9-7 has no overlapping annotation at this time and is thus not reported on in these data.

We filtered the RNA-seq data removing genes which were neither the host genes of the microRNA or members of the Her family. 3 repeats for each stage of development are included in the data and we averaged the expression across the 3

repeats for each stage. The stages reported in the data are based on standard embryonic stages in zebrafish development. However, we wanted to visualize the expression in terms of hours and the stages were converted accordingly. Finally, before plotting these data were z-scored to normalize the expression of each of the genes so that we could compare changes in expression over time rather than absolute levels. These data were then plotted using the heatmap.3 package in R.

N-box / E-box analysis

To assess the number of N and E -box elements in the promoter/proximal enhancer region of the transcriptional start site (TSS) of the microRNA host genes/pri-miRs **(Table S4)** we downloaded the *Danio rerio* genome from Ensembl. Using the genome coordinates from (Nepal et al., 2016) (supplementary Table-S4) for the miR-9 TSS we took a region of 2kb upstream to 1kb downstream of the TSS. The N and E-boxes in each region were then counted. The N and E-box sequences can be found in **Table S5**. These data were then plotted using R (R Core, 2019) and the ggplot2 library (Wickham, 2016)

Figure Legends

Figure 1. Pri-miR-9 paralogues are expressed with different temporal onset. (a) Representative example of chromogenic whole mount in situ hybridization (WM-ISH) of miR-9 using miR-9 LNA 5'-Dig observed at different stages during development; longitudinal view, anterior to the left. Green arrow: forebrain (fb) expression. Blue arrow: hindbrain (hb) expression. **(b)** Chromogenic WM-ISH (Cro-WMISH) of different pri-miR-9s using specific probes for each paralogue observed at different stages during development; longitudinal view, anterior to the left. Blue arrowhead:

expression in hb at 30-31hpf, light blue arrowhead: expression in hb at 34-36hpf, blue arrow: expression in hb at 48hpf. **(c)** High magnification of hb region from respective paralogue at 30-31hpf. (**d)** Heatmap plot representing expression levels in hindbrain; grade 0= no expression in hindbrain, grade 1= weak expression in hindbrain (rhombomere 1 or 2), grade 2= distinct expression in hb and grade 3= strong expression in hb.

Figure 2. Partially overlapping expression of pri-mIR-9s. (a, b) Representative example of double Fluorescent WM-ISH (WM-FISH) labelling of pri-miR-9-1/pri-miR-9-4 **(a)** and pri-miR-9-1/pri-miR-9-5 **(b)** in hindbrain, coronal view, from wild-type embryo observed at 32hpf; merged images (**a, b;** bottom panel) indicate pri-miR-9-4**(a**; magenta**)** and pri-miR-9-5 **(b**; magenta**)** are expressed along the antero-posterior axis while pri-miR-9-1 is limited to anterior hindbrain (**a, b;** green, red arrows). Annotation denotate hindbrain (HB). **(c)** Pixel intensity mean of pri-miR-9-1, pri-miR-9-4 and pri-miR-9-5 observed in ROI (region of interest), delineated by the yellow rectangle in **(a)** and **(b).** Error bar in Scatter dot plot represent mean and SEM of 32-34hpf pri-miR-9-1 (28 slices, 6 embryos), 32-34hpf pri-miR-9-4 (8 slices, 3 embryos) and 32-34hpf pri-miR-9-5 (18 slices, 3 embryos). Kruskal-Wallis with Dunn's multiple comparison test, significance: $p<0.05$*, $p<0.0001$****. **(d, e)** Representative example of double WM-FISH labelling of pri-miR-9-1/pri-miR-9-4 **(d)** and pri-miR-9-1/pri-miR-9-5 **(e)** in hindbrain rhombomere 4 (r4), transversal view, from wild-type embryo observed at 32hpf; merged images (**d, e;** right panel) indicate pri-miR-9-4**(d**; magenta**)** and pri-miR-9-5 **(e**; magenta**)** are expressed in the ventricular zone region while pri-miR-9-1 is almost absent (**d, e;** green). Scale bar 30 µm. **(f)** Schematic representation of transverse section from 32hpf zebrafish

hindbrain at the level of the otic vesicle. VZ: ventricular zone, region where most of progenitor cells are located. MZ: mantle zone, region of ongoing neurogenesis. Within the VZ there are dorsal progenitors (DP), medial progenitors (MP) and ventral progenitors (VP).

Figure 3. Progressive additive expression of pri-miR-9s. (a, b) Representative example of double WM-FISH labelling of pri-miR-9-1 (left panel) and pri-miR-9-4 (middle panel) in hindbrain from wild-type embryo observed at 48hpf, coronal view **(a)** and transversal view **(b). (c, d)** Representative example of double WM-FISH labelling of pri-miR-9-1 (left panel) and pri-miR-9-5 (middle panel) in hindbrain from wild-type embryo observed at 48hpf, coronal view **(c)** and transversal view **(d)**; merged images in coronal view **(a, c; right)** shows overlapping expression of the primary transcripts yet in transversal view **(b, d; right)** reveals distinct expression, pri-miR-9-1 is expressed more broadly toward the dorsal progenitor region. Scale bar 30μm. hb: hindbrain **(e)** Schematic representation of transverse section from 48hpf zebrafish hindbrain at the level of the otic vesicle. VZ: ventricular zone, region where most of progenitor cells are located. MZ: mantle zone/marginal zone, region of ongoing neurogenesis and mature neurons. Within the VZ there are dorsal progenitors (DP), medial progenitors (MP) and ventral progenitors (VP).

Figure 4. mature miR-9 produced by overlapping activation of distinct miR-9 loci. (a-d) Representative example of double WM-FISH labelling pri-miR-9-1 and pri-miR-9-4 combined with cell boundary staining, BODIPY-texas red (BP-TR). **(b)** Indicates cells expressing both, pri-miR-9-1 (green) and pri-miR-9-4 (magenta). **(c)** Indicates cells expressing only pri-miR-9-1 (green). **(d)** Indicates cells expressing

only pri-miR-9-4 (magenta). **(e-h)** Representative example of double WM-FISH labelling pri-miR-9-1 and pri-miR-9-5 combined with BP-TR. **(f)** Indicates cells expressing both, pri-miR-9-1 (green) and pri-miR-9-5 (magenta). **(g)** Indicates cells expressing only pri-miR-9-1 (green). **(h)** Indicates cells expressing only pri-miR-9-5 (magenta). Images were acquired from hindbrain r4, transversal sections, from 48hpf wild-type embryos. Scale bars 30µm and 5µm.

Figure 5. Diverse regulation of miR-9 promoters. (a) Bar plot showing the number of N (green) and E (blue) boxes around the TSS (2kb upstream, 1kb downstream) of the miR-9 genes. **(b)** Scatter plot showing the relationship between the number of N boxes and E boxes around the TSS (2kb upstream, 1kb downstream) of the miR-9 genes**. (c)** Representative example of double WM-FISH labelling *her9* (green) and *her6* (magenta) in hindbrain, transversal view, from wild-type embryo observed at 44hpf, white line indicates dorsal and medial progenitor region. Scale bar 30µm. **(d,e)** Representative example of double WM-FISH labelling pri-miR-9-1 (green)/pri-miR-9-4 (magenta) **(d)** and pri-miR-9-1 (green)/pri-miR-9-5 (magenta) **(e)** in hindbrain, transversal view, from wild-type embryos observed at 48hpf. Dashed white line indicates ventral progenitor region. Scale bar 30µm.

REFERENCE

Akazawa, C., Sasai, Y., Nakanishi, S., and Kageyama, R. (1992). Molecular characterization of a rat negative regulator with a basic helix-loop-helix structure predominantly expressed in the developing nervous system. J Biol Chem *267*, 21879-21885.

Alwin Prem Anand, A., Huber, C., Asnet Mary, J., Gallus, N., Leucht, C., Klafke, R., Hirt, B., and Wizenmann, A. (2018). Expression and function of microRNA-9 in the mid-hindbrain area of embryonic chick. BMC Dev Biol *18*, 3.

Amores, A., Force, A., Yan, Y.L., Joly, L., Amemiya, C., Fritz, A., Ho, R.K., Langeland, J., Prince, V., Wang, Y.L.*, et al.* (1998). Zebrafish hox clusters and vertebrate genome evolution. Science *282*, 1711-1714.

Bonev, B., Pisco, A., and Papalopulu, N. (2011). MicroRNA-9 reveals regional diversity of neural progenitors along the anterior-posterior axis. Dev Cell *20*, 19-32.

Bonev, B., Stanley, P., and Papalopulu, N. (2012). MicroRNA-9 Modulates Hes1 ultradian oscillations by forming a double-negative feedback loop. Cell Rep *2*, 10-18.

Chen, P.Y., Manninga, H., Slanchev, K., Chien, M., Russo, J.J., Ju, J., Sheridan, R., John, B., Marks, D.S., Gaidatzis, D.*, et al.* (2005). The developmental miRNA profiles of zebrafish as determined by small RNA cloning. Genes Dev *19*, 1288-1293.

Coolen, M., Katz, S., and Bally-Cuif, L. (2013). miR-9: a versatile regulator of neurogenesis. Frontiers in cellular neuroscience *7*, 220.

Coolen, M., Thieffry, D., Drivenes, O., Becker, T.S., and Bally-Cuif, L. (2012). miR-9 controls the timing of neurogenesis through the direct inhibition of antagonistic factors. Dev Cell *22*, 1052-1064.

Dessaud, E., Yang, L.L., Hill, K., Cox, B., Ulloa, F., Ribeiro, A., Mynett, A., Novitch, B.G., and Briscoe, J. (2007). Interpretation of the sonic hedgehog morphogen gradient by a temporal adaptation mechanism. Nature *450*, 717-720.

Dubaissi, E., Panagiotaki, N., Papalopulu, N., and Vize, P.D. (2012). Antibody development and use in chromogenic and fluorescent immunostaining. Methods Mol Biol *917*, 411-429.

Galant, S., Furlan, G., Coolen, M., Dirian, L., Foucher, I., and Bally-Cuif, L. (2016). Embryonic origin and lineage hierarchies of the neural progenitor subtypes building the zebrafish adult midbrain. Dev Biol *420*, 120-135.

Goodfellow, M., Phillips, N.E., Manning, C., Galla, T., and Papalopulu, N. (2014). microRNA input into a neural ultradian oscillator controls emergence and timing of alternative cell states. Nature communications *5*, 3399.

Hafner, A., Reyes, J., Stewart-Ornstein, J., Tsabar, M., Jambhekar, A., and Lahav, G. (2020). Quantifying the Central Dogma in the p53 Pathway in Live Single Cells. Cell Syst *10*, 495-505 e494.

Hirata, H., Yoshiura, S., Ohtsuka, T., Bessho, Y., Harada, T., Yoshikawa, K., and Kageyama, R. (2002). Oscillatory expression of the bHLH factor Hes1 regulated by a negative feedback loop. Science *298*, 840-843.

Jaillon, O., Aury, J.M., Brunet, F., Petit, J.L., Stange-Thomann, N., Mauceli, E., Bouneau, L., Fischer, C., Ozouf-Costaz, C., Bernot, A.*, et al.* (2004). Genome duplication in the teleost fish Tetraodon nigroviridis reveals the early vertebrate proto-karyotype. Nature *431*, 946-957.

Kim, C.K., Asimes, A., Zhang, M., Son, B.T., Kirk, J.A., and Pak, T.R. (2020). Differential Stability of miR-9-5p and miR-9-3p in the Brain Is Determined by Their Unique Cis- and Trans-Acting Elements. eNeuro *7*.

Kozomara, A., Birgaoanu, M., and Griffiths-Jones, S. (2019). miRBase: from microRNA sequences to function. Nucleic Acids Res *47*, D155-D162.

Lea, R., Bonev, B., Dubaissi, E., Vize, P.D., and Papalopulu, N. (2012). Multicolor fluorescent in situ mRNA hybridization (FISH) on whole mounts and sections. Methods Mol Biol *917*, 431-444.

Lyons, D.A., Guy, A.T., and Clarke, J.D. (2003). Monitoring neural progenitor fate through multiple rounds of division in an intact vertebrate brain. Development *130*, 3427-3436.

Marzi, M.J., Ghini, F., Cerruti, B., de Pretis, S., Bonetti, P., Giacomelli, C., Gorski, M.M., Kress, T., Pelizzola, M., Muller, H.*, et al.* (2016). Degradation dynamics of microRNAs revealed by a novel pulse-chase approach. Genome Res *26*, 554-565.

Nepal, C., Coolen, M., Hadzhiev, Y., Cussigh, D., Mydel, P., Steen, V.M., Carninci, P., Andersen, J.B., Bally-Cuif, L., Muller, F.*, et al.* (2016). Transcriptional, post-transcriptional and chromatin-associated regulation of pri-miRNAs, pre-miRNAs and moRNAs. Nucleic Acids Res *44*, 3070-3081.

Novak, B., and Tyson, J.J. (2008). Design principles of biochemical oscillators. Nature reviews Molecular cell biology *9*, 981-991.

R Core, T. (2019). R: A language and environment for statistical computing.

Rodriguez-Otero, P., Roman-Gomez, J., Vilas-Zornoza, A., Jose-Eneriz, E.S., Martin-Palanco, V., Rifon, J., Torres, A., Calasanz, M.J., Agirre, X., and Prosper, F. (2011). Deregulation of FGFR1 and CDK6 oncogenic pathways in acute lymphoblastic leukaemia harbouring epigenetic modifications of the MIR9 family. Br J Haematol *155*, 73-83.

Ruegger, S., and Grosshans, H. (2012). MicroRNA turnover: when, how, and why. Trends Biochem Sci *37*, 436-446.

Sasai, Y., Kageyama, R., Tagawa, Y., Shigemoto, R., and Nakanishi, S. (1992). Two mammalian helix-loop-helix factors structurally related to Drosophila hairy and Enhancer of split. Genes Dev *6*, 2620-2634.

Shibata, M., Kurokawa, D., Nakao, H., Ohmura, T., and Aizawa, S. (2008). MicroRNA-9 modulates Cajal-Retzius cell differentiation by suppressing Foxg1 expression in mouse medial pallium. J Neurosci *28*, 10415-10421.

Shibata, M., Nakao, H., Kiyonari, H., Abe, T., and Aizawa, S. (2011). MicroRNA-9 regulates neurogenesis in mouse telencephalon by targeting multiple transcription factors. J Neurosci *31*, 3407-3422.

Shimojo, H., Ohtsuka, T., and Kageyama, R. (2008). Oscillations in notch signaling regulate maintenance of neural progenitors. Neuron *58*, 52-64.

Soto, X., Biga, V., Kursawe, J., Lea, R., Doostdar, P., Thomas, R., and Papalopulu, N. (2020). Dynamic properties of noise and Her6 levels are optimized by miR-9, allowing the decoding of the Her6 oscillator. EMBO J *39*, e103558.

Tambalo, M., Mitter, R., and Wilkinson, D.G. (2020). A single cell transcriptome atlas of the developing zebrafish hindbrain. Development *147*.

Thisse, C., and Thisse, B. (2008). High-resolution in situ hybridization to whole-mount zebrafish embryos. Nature protocols *3*, 59-69.

Walker, J.C., and Harland, R.M. (2008). Expression of microRNAs during embryonic development of Xenopus tropicalis. Gene Expr Patterns *8*, 452-456.

White, R.J., Collins, J.E., Sealy, I.M., Wali, N., Dooley, C.M., Digby, Z., Stemple, D.L., Murphy, D.N., Billis, K., Hourlier, T.*, et al.* (2017). A high-resolution mRNA expression time course of embryonic development in zebrafish. eLife *6*.

Wickham, H. (2016). ggplot2, Elegant Graphics for Data Analysis (Springer International Publishing).

Wong, S.F., Agarwal, V., Mansfield, J.H., Denans, N., Schwartz, M.G., Prosser, H.M., Pourquie, O., Bartel, D.P., Tabin, C.J., and McGlinn, E. (2015). Independent

regulation of vertebral number and vertebral identity by microRNA-196 paralogs. Proc Natl Acad Sci U S A *112*, E4884-4893.

Yates, A.D., Achuthan, P., Akanni, W., Allen, J., Allen, J., Alvarez-Jarreta, J., Amode, M.R., Armean, I.M., Azov, A.G., Bennett, R.*, et al.* (2020). Ensembl 2020. Nucleic Acids Res *48*, D682-D688.

Zhao, C., Sun, G., Li, S., and Shi, Y. (2009). A feedback regulatory loop involving microRNA-9 and nuclear receptor TLX in neural stem cell fate determination. Nat Struct Mol Biol *16*, 365-371.

Zhao, J., Lin, Q., Kim, K.J., Dardashti, F.D., Kim, J., He, F., and Sun, Y. (2015). Ngn1 inhibits astrogliogenesis through induction of miR-9 during neuronal fate specification. eLife *4*, e06885.

Figure 1

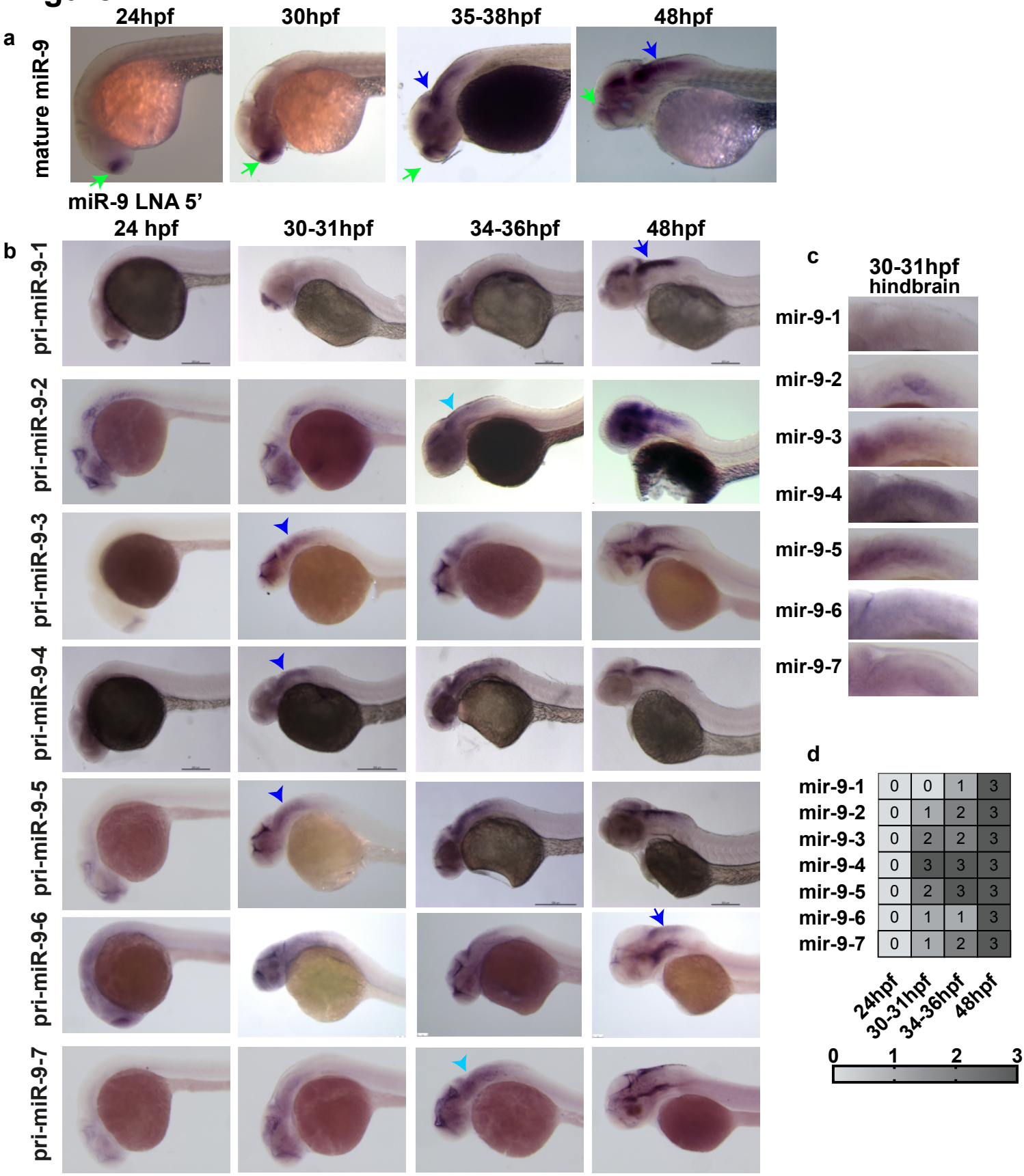
a
24hpf
30hpf
35-38hpf
48hpf
mature miR-9
miR-9 LNA 5'
b
24 hpf
30-31hpf
34-36hpf
48hpf
pri-miR-9-1
pri-miR-9-2
pri-miR-9-3
pri-miR-9-4
pri-miR-9-5
pri-miR-9-6
pri-miR-9-7
c
30-31hpf
hindbrain
mir-9-1
mir-9-2
mir-9-3
mir-9-4
mir-9-5
mir-9-6
mir-9-7
d
mir-9-1 0 0 1 3
mir-9-2 0 1 2 3
mir-9-3 0 2 2 3
mir-9-4 0 3 3 3
mir-9-5 0 2 3 3
mir-9-6 0 1 1 3
mir-9-7 0 1 2 3
24hpf
30-31hpf
34-36hpf
48hpf
0
1
2
3

Figure 2

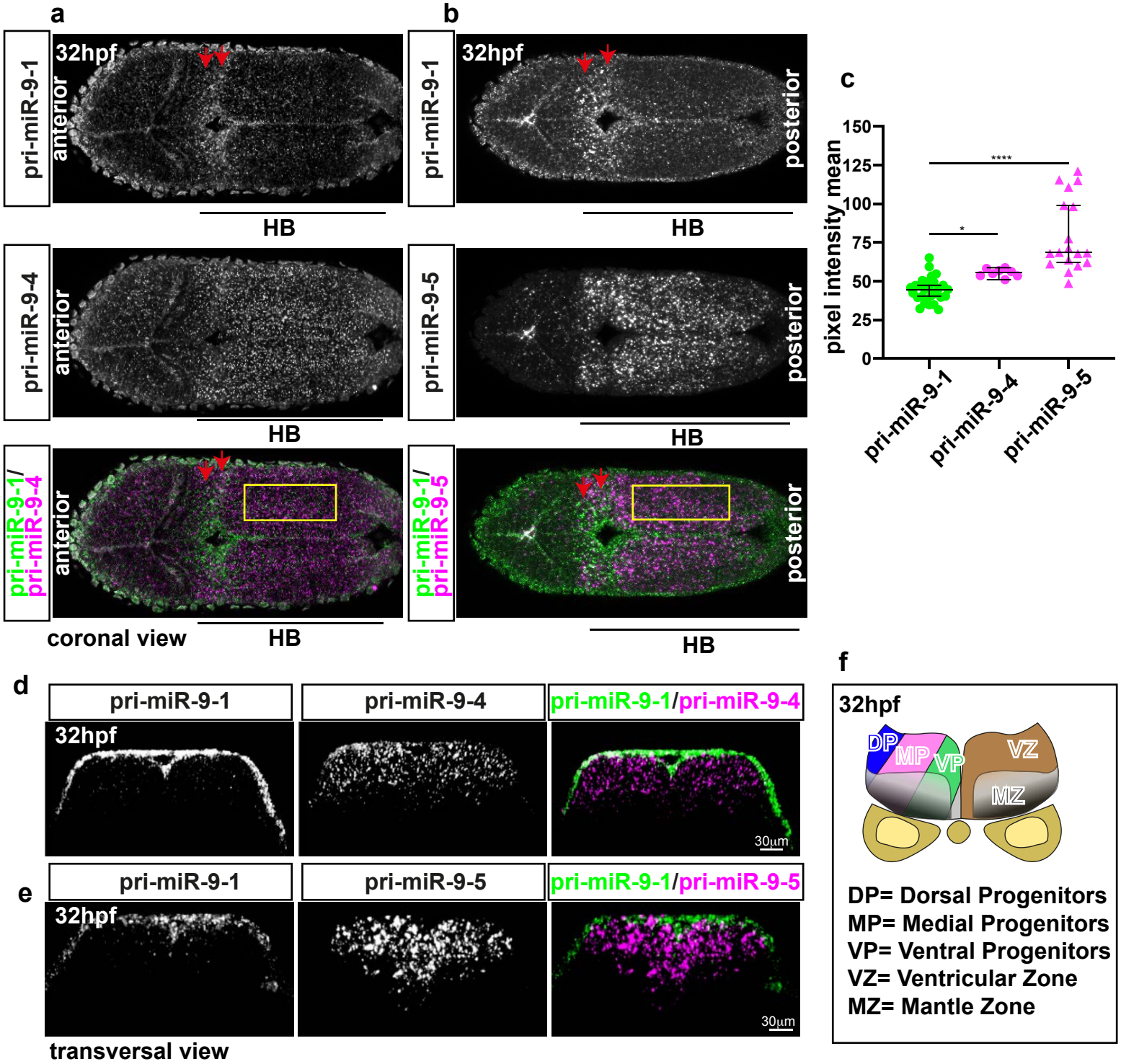
a
b
c
d
e
f
32hpf
pri-miR-9-1
pri-miR-9-4
pri-miR-9-5
pri-miR-9-1/pri-miR-9-4
pri-miR-9-1/pri-miR-9-5
anterior
posterior
HB
coronal view
pixel intensity mean
150
125
100
75
50
25
0
****
*
30µm
transversal view
DP
MP
VP
VZ
MZ
DP= Dorsal Progenitors
MP= Medial Progenitors
VP= Ventral Progenitors
VZ= Ventricular Zone
MZ= Mantle Zone

Figure 3

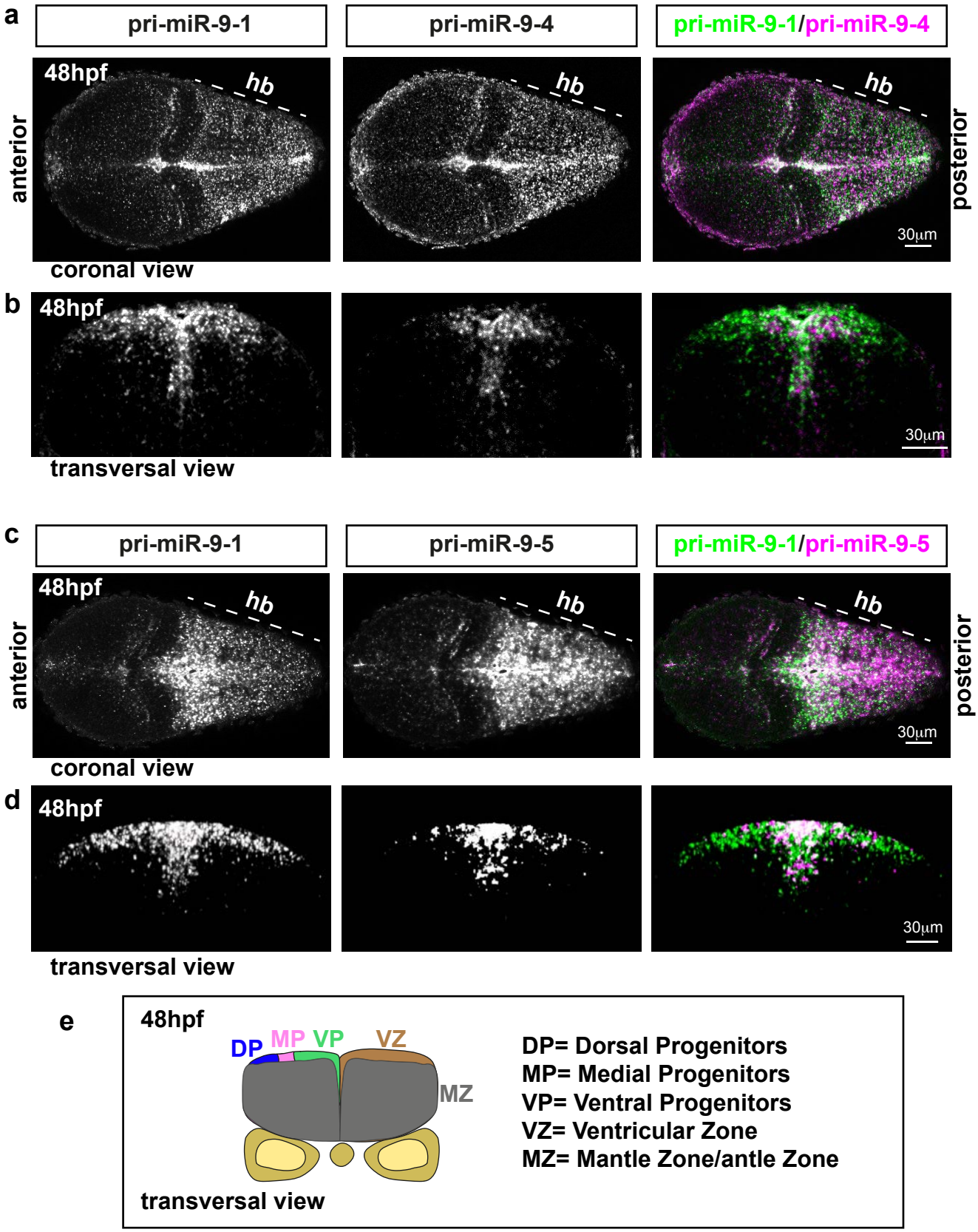
a
pri-miR-9-1
pri-miR-9-4
pri-miR-9-1/pri-miR-9-4
48hpf
hb
anterior
posterior
30µm
coronal view
b
48hpf
30µm
transversal view
c
pri-miR-9-1
pri-miR-9-5
pri-miR-9-1/pri-miR-9-5
48hpf
hb
anterior
posterior
30µm
coronal view
d
48hpf
30µm
transversal view
e
48hpf
DP
MP
VP
VZ
MZ
transversal view
DP= Dorsal Progenitors
MP= Medial Progenitors
VP= Ventral Progenitors
VZ= Ventricular Zone
MZ= Mantle Zone/antle Zone

Figure 4

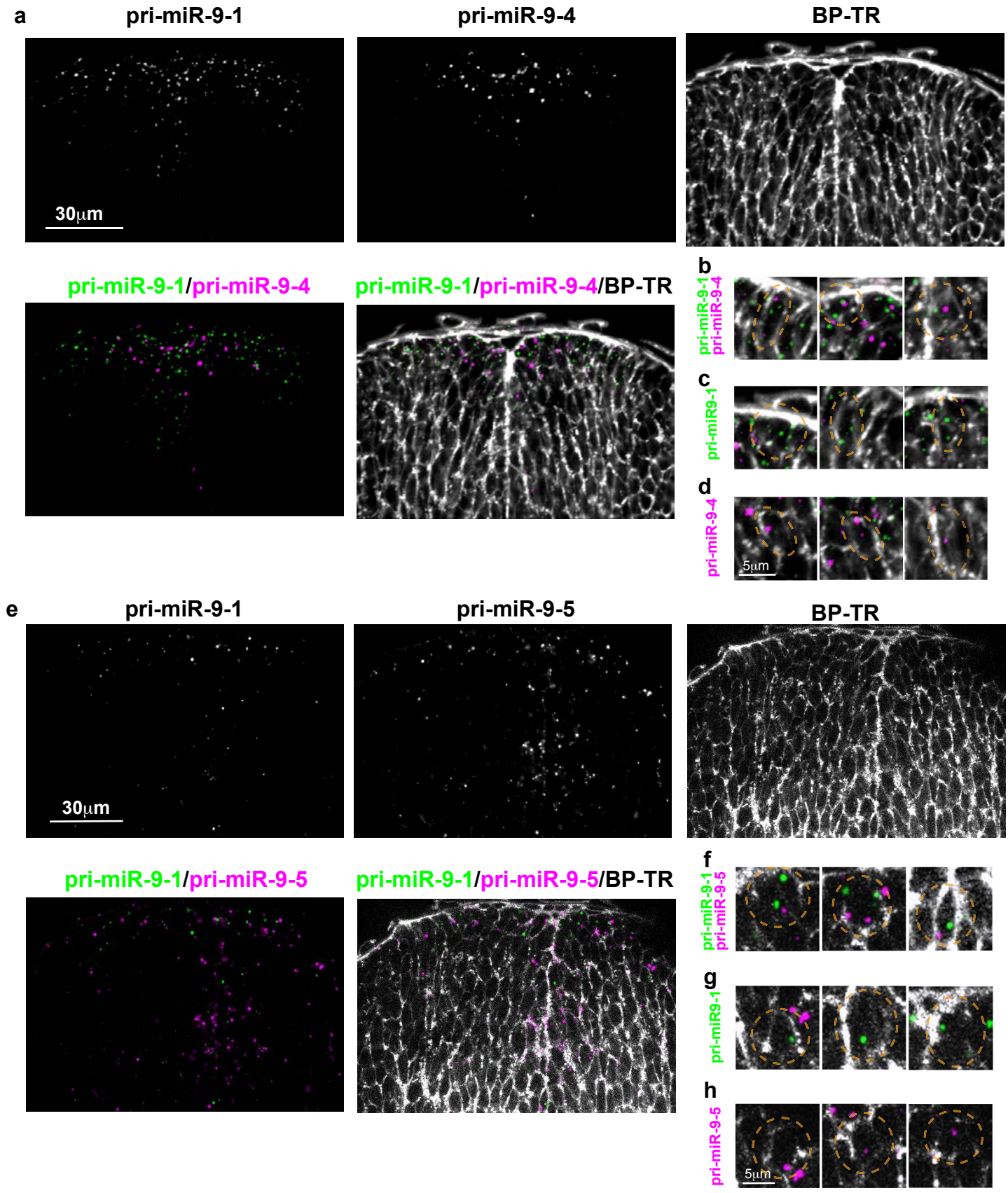
a
pri-miR-9-1
pri-miR-9-4
BP-TR
30μm
pri-miR-9-1/pri-miR-9-4
pri-miR-9-1/pri-miR-9-4/BP-TR
b
pri-miR-9-1
pri-miR-9-4
c
pri-miR9-1
d
pri-miR-9-4
5μm
e
pri-miR-9-1
pri-miR-9-5
BP-TR
30μm
pri-miR-9-1/pri-miR-9-5
pri-miR-9-1/pri-miR-9-5/BP-TR
f
pri-miR-9-1
pri-miR-9-5
g
pri-miR9-1
h
pri-miR-9-5
5μm

Figure 5

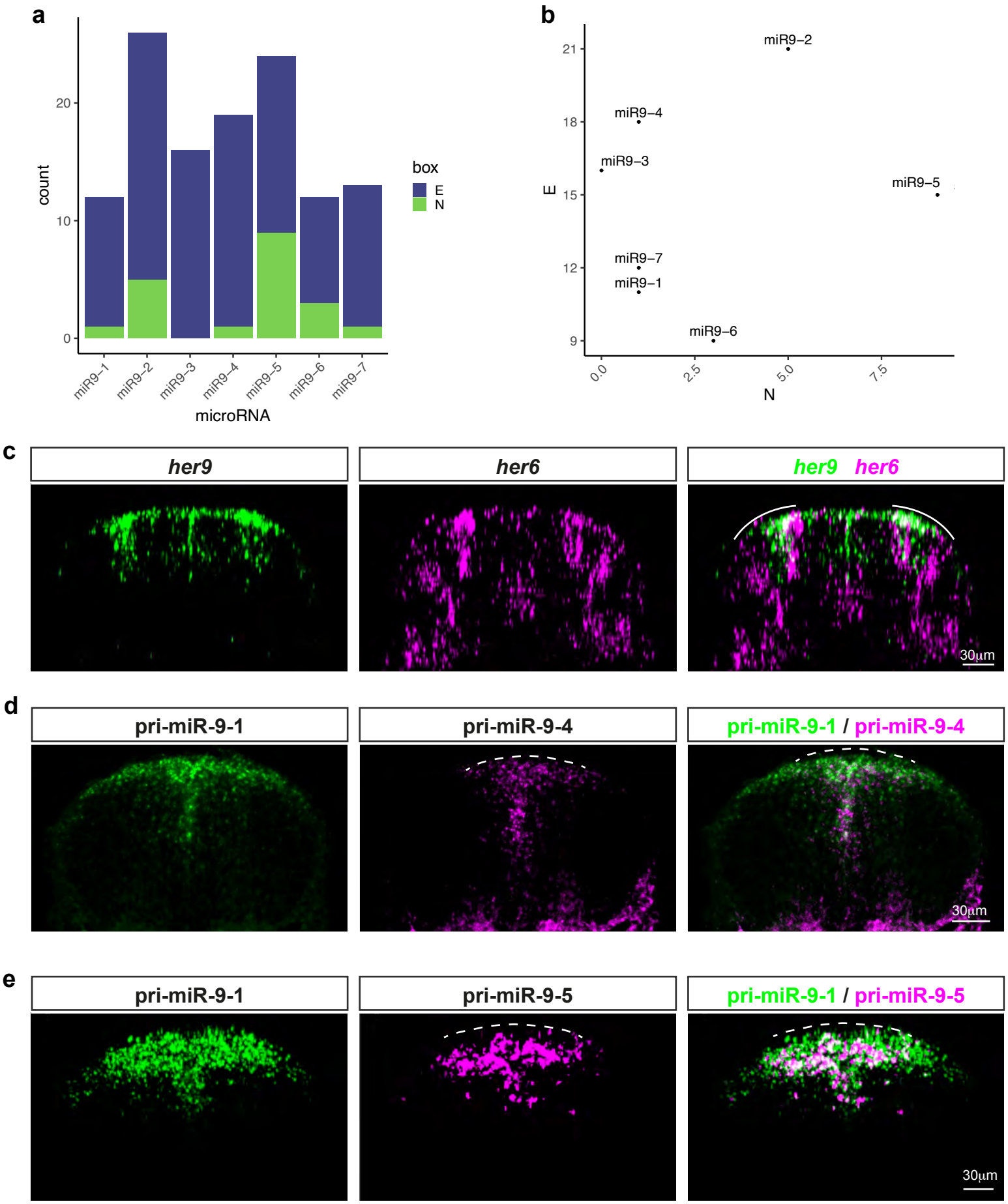
a
count
20
10
0
miR9–1
miR9–2
miR9–3
miR9–4
miR9–5
miR9–6
miR9–7
microRNA
box
E
N
b
E
21
18
15
12
9
miR9–2
miR9–4
miR9–3
miR9–5
miR9–7
miR9–1
miR9–6
0.0
2.5
5.0
7.5
N
c
her9
her6
her9 her6
30μm
d
pri-miR-9-1
pri-miR-9-4
pri-miR-9-1 / pri-miR-9-4
30μm
e
pri-miR-9-1
pri-miR-9-5
pri-miR-9-1 / pri-miR-9-5
30μm